

The Pairing Interaction in the 2D Hubbard Model

T. A. Maier,¹ M. Jarrell,² and D. J. Scalapino³¹Computer Science and Mathematics Division,
Oak Ridge National Laboratory, Oak Ridge, TN 37831-6164²Department of Physics,
University of Cincinnati, Cincinnati, OH 45221⁷³Department of Physics,
University of California, Santa Barbara, CA 93106-9530²
(Dated: May 4, 2021)

A dynamic cluster quantum Monte Carlo approximation is used to study the effective pairing interaction of a 2D Hubbard model with a near-neighbor hopping t and an on-site Coulomb interaction U . The effective pairing interaction is characterized in terms of the momentum and frequency dependence of the eigenfunction of the leading eigenvalue of the irreducible particle-particle vertex. The momentum dependence of this eigenfunction is found to vary as $(\cos k_x - \cos k_y)$ over most of the Brillouin zone and its frequency dependence is determined by the exchange energy J . This implies that the effective pairing interaction is attractive for singlets formed between near-neighbor sites and retarded on a time scale set by J^{-1} . The strength of the pairing interaction measured by the size of the d -wave eigenvalue peaks for U of order the bandwidth $8t$. It is found to increase as the system is underdoped.

I. INTRODUCTION

Results from numerical studies suggest that the two-dimensional (2D) Hubbard model exhibits the basic phenomena which are seen in the high- T_c cuprate materials. At half-filling, one finds a groundstate with long-range antiferromagnetic order¹. Doped away from half-filling there is a pseudogap region^{2,7}, and at low temperature a striped phase^{8,9} as well as d -wave pairing¹⁰. In addition, the various phases appear delicately balanced with respect to changes in parameters. All of these features remind one of the actual cuprate materials, so that it is of interest to understand the structure of the interaction that leads to $d_{x^2-y^2}$ -wave pairing in this model.

Here we will study this interaction for a 2D Hubbard model¹¹ on a square lattice which contains a one-electron near-neighbor hopping t and an onsite Coulomb interaction U . In this case the results depend upon just two parameters U/t and the average site occupation ni . Previous work¹² has shown that the pairing interaction with $U/t = 4$ and $ni = 0.85$ increases with momentum transfer, has a Matsubara frequency dependence similar to that of the $Q = (\pi; \pi)$ spin susceptibility and is mediated by a particle-hole $S = 1$ exchange channel. Here we extend this work to explore the pairing interaction for larger values of U/t and various dopings. We are particularly interested in the case in which U is of order of the bandwidth $8t$. In this case, well developed upper and lower Hubbard bands are seen in the single particle density of states

$$N(\omega) = \frac{1}{N} \sum_{\mathbf{k}} \text{Im} G(\mathbf{k}; i\omega_m \rightarrow \omega + i0^+); \quad (1)$$

Fig. 1 shows $N(\omega)$ with $U/t = 8$ for various fillings. These results were obtained from a maximum entropy continuation¹³ of dynamic cluster quantum Monte Carlo

data on a 16 site cluster. At half-filling, Fig. 1a, for $T = t$ one sees broad upper and lower Hubbard bands. Then, as the temperature scale drops below the exchange energy scale $J = 4t^2/U$, two additional structures appear above and below $\omega = 0$. As Preuss et al.¹⁴ first showed, the inner structures arise from the formation of two coherent bands, each of width $2J$ that form as the antiferromagnetic correlations develop. This characteristic Mottn-Hubbard-antiferromagnetic four band structure^{14,15} is clearly seen when U becomes of order or larger than the bandwidth.

Fig. 1b shows $N(\omega)$ for the doped $ni = 0.9$ case. Here the chemical potential has moved down into the lower coherent band and the spectral weight in the upper coherent band has essentially vanished. Nevertheless, the remnants of the upper and lower Hubbard bands remain. Part of the motivation for this study is to examine the structure of the pairing interaction in this parameter regime.

As in our previous work, the pairing interaction χ^{PP} will be calculated using a dynamic cluster quantum Monte Carlo simulation¹⁶. As shown in Fig. 2, χ^{PP} is the irreducible part of the 4-point particle-particle vertex in the zero center of mass and energy channel. Previously, we discussed how one could extract $\chi^{PP}(\mathbf{k}; \mathbf{k}^0) = \chi^{PP}(\mathbf{k}; \mathbf{k}; \mathbf{k}^0; \mathbf{k}^0)$ with $\mathbf{k} = (\mathbf{k}; i\omega_n)$ using a dynamic cluster quantum Monte Carlo simulation.

While we studied χ^{PP} in our earlier work, here we will focus on the momentum and Matsubara frequency dependence of the $d_{x^2-y^2}$ -wave eigenfunction $\chi_d(\mathbf{k}; i\omega_n)$ of the homogeneous particle-particle Bethe-Salpeter equation

$$\frac{T}{N} \sum_{\mathbf{k}^0} \chi^{PP}(\mathbf{k}; \mathbf{k}^0) G_{\sigma}(\mathbf{k}^0) G_{\sigma}(\mathbf{k} - \mathbf{k}^0) = \chi_d(\mathbf{k}; i\omega_n); \quad (2)$$

At low temperatures, $\chi_d(\mathbf{k}; i\omega_n)$ has the largest eigenvalue and this eigenvalue goes to one at $T = T_c$. As

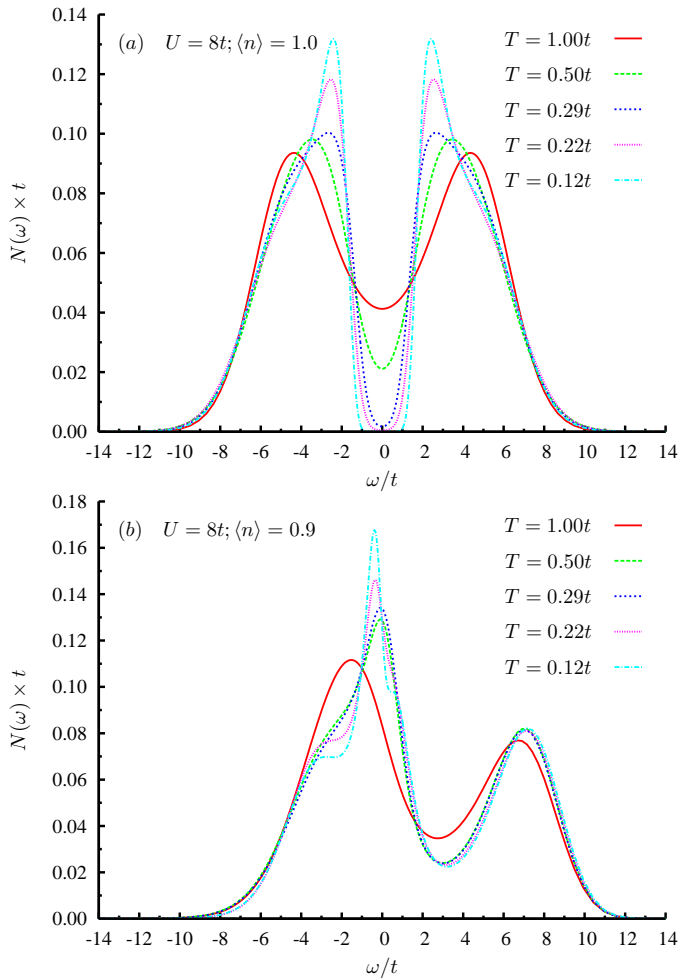


FIG. 1: The single particle density of states $N(\omega)$ versus ω for $U = 8t$, $N_c = 15$ and various values of the temperature T for site fillings of a) $\langle n \rangle = 1.0$, b) $\langle n \rangle = 0.90$.

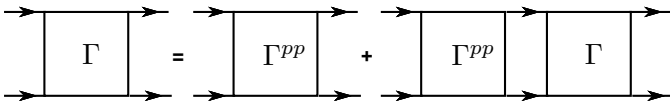


FIG. 2: The Bethe-Salpeter equation for the particle-particle channel showing the relationship between the four-point vertex and the particle-particle irreducible vertex Γ^{pp} . The solid lines are dressed single particle Green's functions.

As T approaches T_c , the momentum and frequency dependence of $\chi_d(\mathbf{k}; !_n)$ reflect the structure of the pairing interaction at T_c , just as the superconducting gap function reflects the \mathbf{k} and $!$ dependence of the pairing interaction in the superconducting state. Thus, while $\chi_d(\mathbf{k}; !_n)$ is not a quantity that is directly measurable, it has a \mathbf{k} -dependence related to the momentum dependence of the interaction and a Matsubara frequency dependence which decays beyond a characteristic frequency associated with the dynamic character of the interaction. It also has the

great advantage of depending upon one momentum and frequency variable as opposed to the multiple momentum and frequency variables of $\chi^{pp}(\mathbf{k}, \mathbf{k}')$.

In the following section II we review the dynamic cluster approximation and discuss how one calculates the $d_{x^2-y^2}$ -wave eigenvalue $\chi_d(T)$ and eigenfunction $\chi_d(\mathbf{k}; !_n)$. Then, in Sec. III we investigate how $\chi_d(T)$ depends upon U and $\langle n \rangle$. Following this, we examine the \mathbf{k} -dependence of $\chi_d(\mathbf{k}; !_n)$ and see how closely it follows the simple $\cos(k_x) \cos(k_y)$ dependence. If it were of this form over the entire Brillouin zone, then it would imply a strictly near-neighbor pairing interaction. Then we turn to the $!$ -dependence which reflects the dynamics of the pairing interaction and study its dependence on U . In Sec. IV, based upon the results for $\chi_d(\mathbf{k}; !_n)$, we construct a simple separable representation of $\chi^{pp}(\mathbf{k}, \mathbf{k}')$ and discuss the strength of the pairing interaction. Sec. V contains our conclusions.

II. THE DYNAMICAL CLUSTER APPROXIMATION

The Dynamical Cluster Approximation (DCA)¹⁶ maps the bulk lattice to a finite size cluster embedded in a self-consistent bath designed to represent the remaining degrees of freedom. Short-range correlations within the cluster are treated explicitly, while the longer-ranged physics is described by a mean-field. By increasing the cluster size, the DCA systematically interpolates between the single-site dynamical mean-field result and the exact result, while remaining an approximation to the thermodynamic limit for finite cluster size.

The essential assumption is that short-range quantities, such as the single-particle self-energy Σ , and its functional derivatives, the two-particle irreducible vertex functions, are well represented as diagrams constructed from a coarse-grained propagator G . To define G , the Brillouin zone in two dimensions is divided into $N_c = L^2$ cells of size $2\pi/L^2$. As illustrated in Fig. 3, each cell is represented by the cluster momentum \mathbf{K} in its center. The coarse-grained Green function $G(\mathbf{K})$ is then obtained from an average over the N_c wave-vectors \mathbf{K} within the cell surrounding \mathbf{K} ,

$$G(\mathbf{K}; !_n) = \frac{N_c}{N} \sum_{\mathbf{K}} \frac{1}{i!_n - \epsilon_{\mathbf{K}+\mathbf{K}'} + \Sigma_c(\mathbf{K}; !_n)} \quad (3)$$

Here the self-energy for the bulk lattice $\Sigma(\mathbf{K} + \mathbf{K}'; !_n)$ has been approximated by the cluster self-energy $\Sigma_c(\mathbf{K}; !_n)$. Consequently, the compact Feynman diagrams constructed from $G(\mathbf{K}; !_n)$ collapse onto those of an effective cluster problem embedded in a host which accounts for the fluctuations arising from the hybridization between the cluster and the rest of the system. The non-interacting part of the effective cluster action is then defined by the cluster-excluded inverse Green's function

$$G^{-1}(\mathbf{K}; !_n) = G^{-1}(\mathbf{K}; !_n) + \Sigma_c(\mathbf{K}; !_n) \quad (4)$$

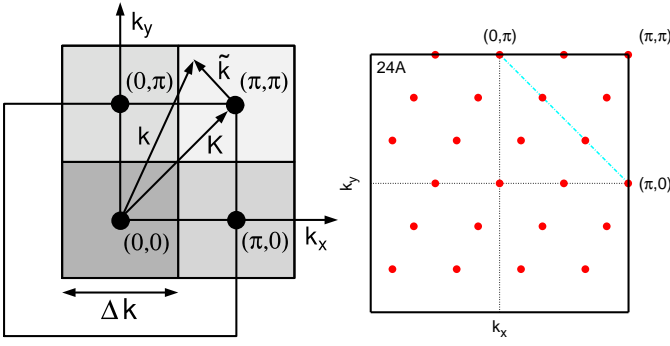


FIG. 3: In the DCA the Brillouin zone is divided into N_c cells each represented by a cluster momentum K . Irreducible quantities such as the single-particle self-energy and two-particle irreducible vertex are constructed from coarse-grained propagators $G_c(K)$ that are averaged over the momentum k^0 within the cell represented by K . The cluster momenta K for a 4-site cluster are shown on the left and those for a 24-site cluster on the right.

which accounts for the hybridization between the cluster and the host. Given $G_c(K; !_n)$ and the interaction on the cluster $U_{i_1 n_1 i_2 n_2}$, one can then set up a Hirsch-Fye quantum Monte Carlo algorithm¹⁷ to calculate the cluster Green function and from it the cluster self-energy $\Sigma_c(K; !_n)$ which is used in Eq. (3) to re-calculate the coarse-grained Green function $G_c(K; !_n)$ ^{16,18}. This process is then iterated to convergence.

Since a determinantal Monte Carlo method is used, there is also a sign problem for the doped Hubbard model. However, the coupling of the cluster to the self-consistent host significantly reduce the sign problem so that lower temperatures can be reached¹⁸.

The DCA cluster one- and two-particle Green's functions that we calculate have the standard finite temperature definitions

$$G_c(K_2; X_1) = \frac{1}{T} \langle c(X_2) c^\dagger(X_1) \rangle \quad (5a)$$

and

$$G_{c2}(K_4; X_3; X_2; X_1) = \frac{1}{T} \langle c_4(X_4) c_3(X_3) c_2^\dagger(X_2) c_1^\dagger(X_1) \rangle \quad (5b)$$

Here, $X_i = (X_i; \tau_i)$, where X_i denotes a site in the DCA cluster, τ_i the imaginary time, T is the usual inverse ordering operator, and $c^\dagger(X_2)$ creates a particle on the cluster with spin \uparrow . Fourier transforming on both the cluster space and imaginary time variables gives $G_c(K)$ and $G_{c2}(K_4; K_3; K_2; K_1)$ with $K = (K; i!_n)$. Using $G_c(K)$ and $G_{c2}(K_4; K_3; K_2; K_1)$, one can extract the cluster four-point vertex from

$$G_{c2}(K_4; K_3; K_2; K_1) = G_c(K_1) G_c(K_2) [K_1; K_4; K_2; K_3; K_1; K_3; K_2; K_4] + \frac{T}{N} \sum_{K_1+K_2+K_3+K_4} G_c(K_4) G_c(K_3) G_c(K_2) G_c(K_1) \quad (6)$$

Then, using G_c and G_{c2} , one can determine the irreducible particle-particle vertex Γ^{pp} from the Bethe-Salpeter equation shown in Fig. 2.

Using Γ^{pp} , the eigenvalues and eigenfunctions of the Bethe-Salpeter equation may then be calculated from

$$\frac{T}{N} \sum_{K^0} \Gamma^{pp}(K; K; K^0; K^0) G_c(K^0) G_\#(K^0) \Gamma^{pp}(K^0) = \Gamma^{pp}(K) \quad (7)$$

Here, the sum over k^0 denotes a sum over both momentum k^0 and Matsubara $i!_n$ variables. We decompose $k^0 = K^0 + K^0$. By assumption, irreducible quantities like Γ^{pp} and $G_\#$ do not depend on K^0 , allowing us to coarse-grain the Green function legs, yielding an equation that depends only on coarse-grained and cluster quantities

$$\frac{T}{N_c} \sum_{K^0} \Gamma^{pp}(K; K; K^0; K^0) \Gamma^{pp}(K^0) \Gamma^{pp}(K^0) = \Gamma^{pp}(K) \quad (8)$$

with $\Gamma^{pp}_0(K^0) = \frac{N_c}{N} \sum_{K^0} G_c(K^0 + K^0; i!_n) G_\#(K^0; i!_n)$.

Here, we show a number of results for the 4-site cluster shown on the left in Fig. 3, which allows us to investigate larger values of U and lower temperatures than the 24-site cluster. As discussed in Ref.¹⁰, the 4-site cluster does not allow for the effect of paired phase fluctuations. Simulations on the 24-site cluster were used to determine the k dependence of $\chi_d(k; !_n)$.

III. THE STRUCTURE OF THE PAIRING INTERACTION AS REFLECTED IN $\chi_d(T)$ AND $\chi_d(k; !_n)$

The temperature dependence of the d -wave eigenvalues $\chi_d(T)$ calculated using a 4-site cluster for a filling $\nu = 0.9$ with $U=t = 4, 8$ and 12 are shown in Fig. 4a. Fig. 4b shows χ_d versus $U=t$ for $T = 0.15t$. Here one sees that it is favorable to have a Coulomb interaction strength U of order the bandwidth $8t$. This is consistent with the notion that it is important to have strong short-range antiferromagnetic correlations. However, because the exchange interaction $J = 4t^2/U$ at strong coupling, the short-range antiferromagnetic correlations decrease when U becomes large compared to the bandwidth.

The dependence of $\chi_d(T)$ on the filling ν is illustrated in Fig. 5 for $U=t = 6$. What one sees is that $\chi_d(T)$ increases as the system is doped towards half-filling. However, at half-filling the dominant eigenvalue of the 4-point vertex occurs in the $Q = (\pi; \pi)$ irreducible particle-hole $S = 1$ channel as indicated by the dashed line in Fig. 5, and the groundstate at $T = 0$ has long-range antiferromagnetic order.

For $\nu = 0.9$ and $U=t = 8$, the momentum dependence of the d -wave eigenvector $\chi_d(K; !_n)$ for the 24-site cluster at $\nu = T$ is shown in Fig. 6. Here, for $T=t = 0.22$,

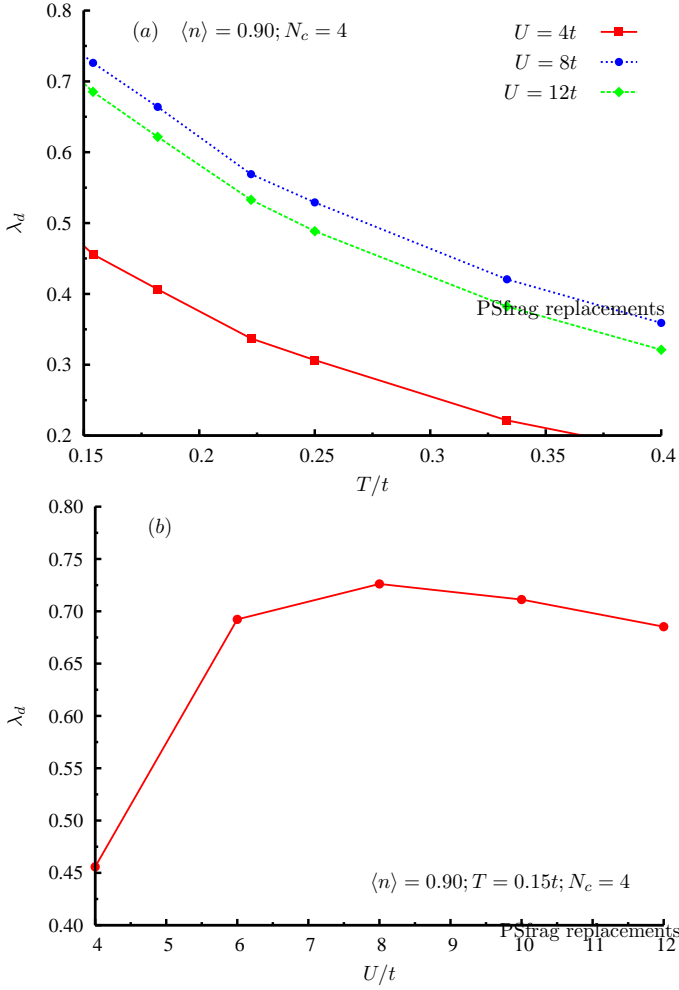


FIG. 4: (a) The $d_{x^2-y^2}$ eigenvalue $\lambda_d(T)$ versus $T=t$ for $U = 4t, 8t$ and $12t$ and $\langle n \rangle = 0.90$. (b) The $d_{x^2-y^2}$ eigenvalue $\lambda_d(T)$ versus $U=t$ for $T = 0.15t$ and $\langle n \rangle = 0.90$.

$\lambda_d(T) = 0.42$ and the values of K lay along the dashed line shown in Fig. 3. One clearly sees the d-wave structure of λ_d . The dependence of $\lambda_d(K; T)$ for K along the K_x axis is shown in the inset of Fig. 6. Here, one sees that $\lambda_d(K; T)$ falls off as K moves away from the Fermi surface towards the zone center.

We have also calculated the projection of $\lambda_d(K; T)$ on the first and second $d_{x^2-y^2}$ crystal harmonics

$$d_i = \sum_K g_i(K) \lambda_d(K; T) \quad (9)$$

with $g_1(K) = \cos K_x - \cos K_y$ and $g_2(K) = \cos 2K_x - \cos 2K_y$. In table I, we list the values of $d_2=d_1$ versus U at a filling $\langle n \rangle = 0.9$. Here the sum in Eq. (9) is over the entire Brillouin zone and the temperature was adjusted so that the d-wave eigenvalue λ_d for each $U=t$ was the same ($\lambda_d = 0.4$). If the sum over K in Eq. (9) is restricted to values which lay along the dashed line in Fig. 3, this ratio vanishes exactly in the 24-site cluster,

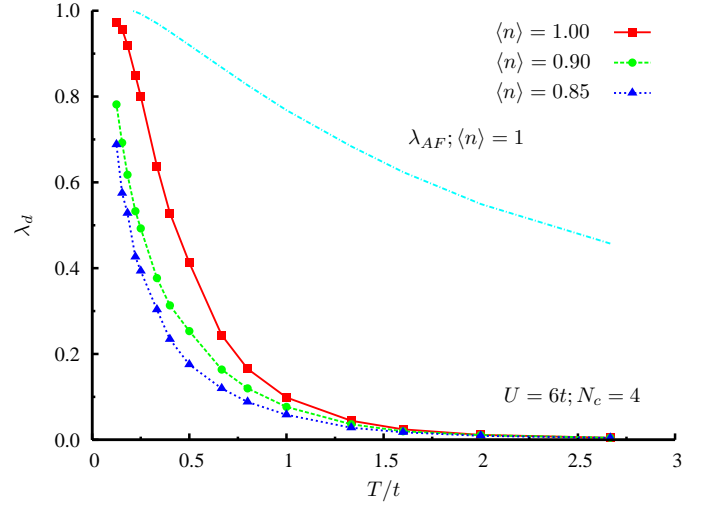


FIG. 5: The $d_{x^2-y^2}$ eigenvalue $\lambda_d(T)$ versus $T=t$ for various band fillings $\langle n \rangle$ for $U=t = 6$. The dashed line represents the leading eigenvalue λ_{AF} in the $Q = (\pi; \pi), S = 1$ particle-hole channel at half-filling.

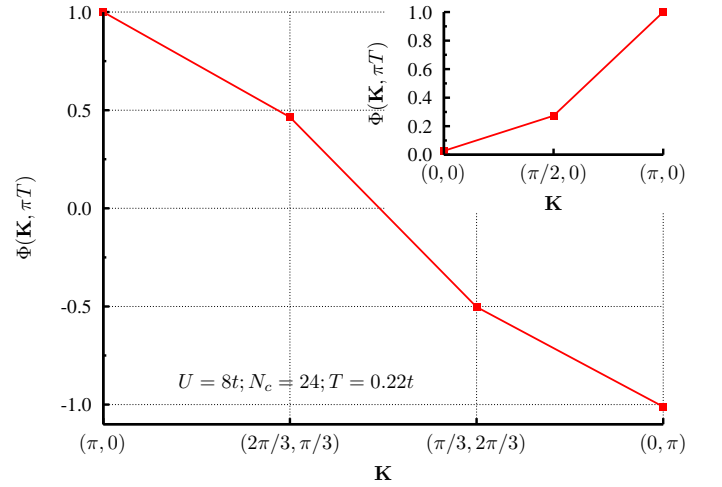


FIG. 6: The $d_{x^2-y^2}$ eigenvector $\lambda_d(K; \langle n \rangle)$ at $\langle n \rangle = T$, normalized to its value at $K = (\pi; 0)$, versus K for $U=t = 8$, band filling $\langle n \rangle = 0.9$ and $T=t = 0.22$. In the main figure, the K points move along the dashed line shown in Fig. 3. The inset shows the behavior of λ_d when K varies along the k_x axis.

since $g_2(K) = 0$ on the momenta K along the dashed line.

$U=t$	4	6	8
$d_2=d_1$	0.064	0.128	0.157

TABLE I: The ratio of the second to the first crystal d-wave harmonic projection of $\lambda_d(K; T)$ for $\langle n \rangle = 0.9$ and $\lambda_d = 0.4$.

The Matsubara frequency dependence of $\lambda_d(K; \langle n \rangle) = \lambda_d(K; T)$ with $K = (\pi; 0)$ is shown in Fig. 7 for $\langle n \rangle = 0.9$ and $U=t = 4, 8$ and 12 . Also shown

in each case is the frequency dependence of $\langle Q; !_n \rangle$ with $Q = (\pi; 0)$. The decrease of the characteristic exchange energy as $U=t$ increases is seen in Figs. 7a(c). It is clear from these results that the dynamics of the pairing interaction PP , reflected in the $!_n$ dependence of $\langle d(k; !_n) \rangle$, is associated with the spin-fluctuation spectrum.

IV. A SEPARABLE REPRESENTATION OF THE PAIRING INTERACTION

With the results obtained for the d-wave eigenvector $\langle d(K) \rangle$, one can construct a simple separable representation of the pairing interaction $\text{PP}(K; K^0)$

$$\text{PP}(K; K^0) = V_d \langle d(K) \rangle \langle d(K^0) \rangle : \quad (10)$$

Using this separable form for $\text{PP}(K; K^0)$, one finds that Eq. (8) gives

$$V_d \frac{T}{N_c} \sum_{K^0} \langle d(K^0) \rangle \text{PP}(K; K^0) = \langle d(K) \rangle : \quad (11)$$

Then, using the dressed DCA Monte Carlo single particle Green's functions and the DCA results for $\langle d \rangle$, we can determine the strength V_d of the separable interaction from Eq. (11). The strength of V_d depends upon both the site occupation hni and the temperature T . An alternative way of extracting a simple approximation for the pairing interaction is to use the d-wave projected irreducible vertex for $!_n = !_{n^0} = T$

$$V_d^{(T)} = \frac{1}{N_c} \sum_{K; K^0} g(K) \text{PP}(K; T; K^0; T) g(K^0) \quad (12)$$

with $g(K) = (\cos K_x - \cos K_y) = 2$.

Fig. 8 shows $V_d(T)$ and $V_d^{(T)}(T)$ for $U = 8t$ and various values of the site occupation hni . Both approximations give very similar results. It is interesting to see that V_d becomes stronger as hni approaches half-filling. This is characteristic of the Motz-Hubbard system and has been previously observed. A determinantal quantum Monte Carlo calculation of the d-wave eigenvalue on an 8×8 lattice at half-filling with $U = 8t$ found that $\langle d \rangle$ approached 1 as the temperature was lowered¹⁹. As noted there, in this case the antiferromagnetic eigenvalue remained dominant and on an infinite lattice the groundstate would have long-range antiferromagnetic order at $T = 0$. A related behavior is seen for the two-leg ladder, where the pair binding energy of a finite ladder is greatest for the first two holes that are added²⁰. This latent pairing tendency of the half-filled Hubbard model is also seen in the magnitude of the probability amplitude for adding two near-neighbor holes in a d-wave state reported by Plekhanov et al.²¹.

Although V_d increases as hni goes to 1, the number of holes that are available for pairing is suppressed as is T_c .

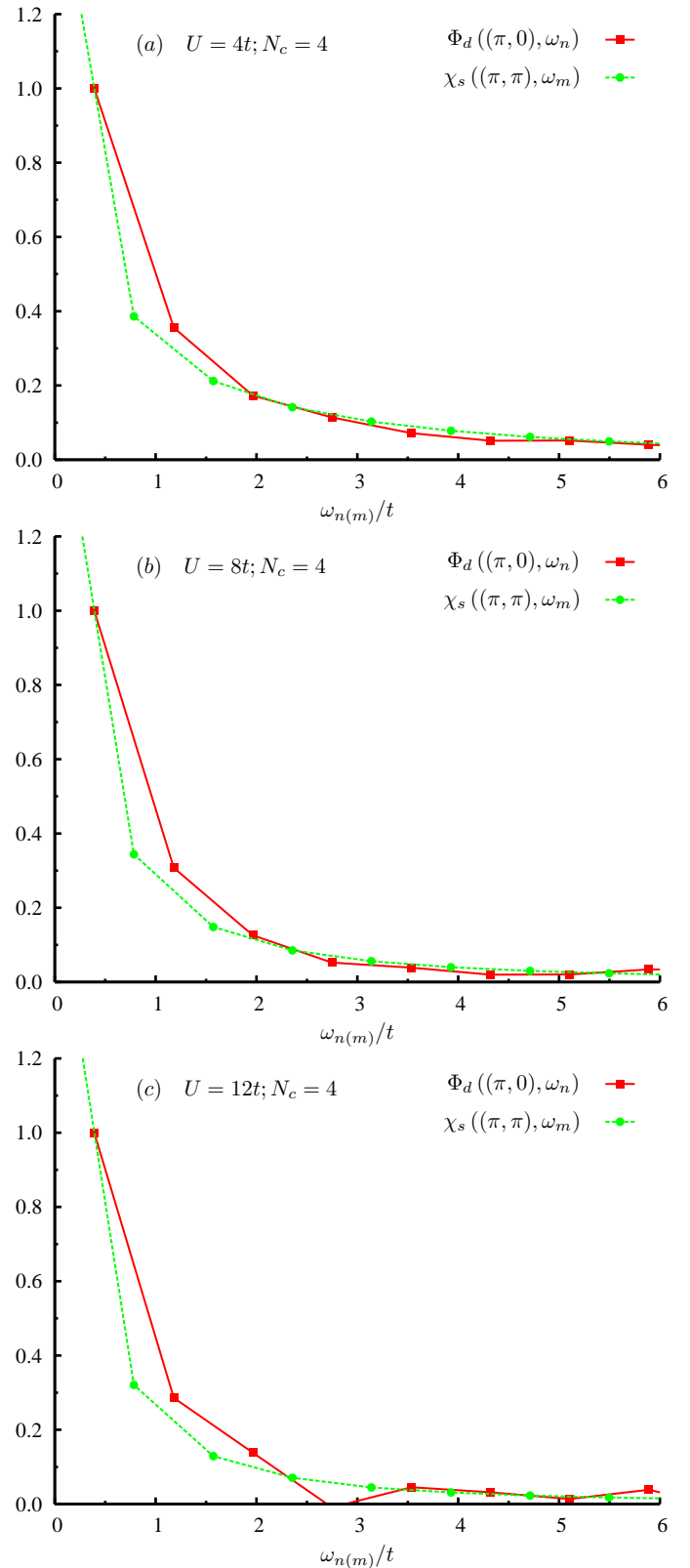


FIG. 7: The Matsubara frequency dependence of $\langle d(K; !_n) \rangle = \langle d(K; T) \rangle$ with $K = (\pi; 0)$ for (a) $U=t = 4$, (b) $U=t = 8$ and (c) $U=t = 12$ calculated for $N_c = 4$. Here $!_n = (2n + 1)T$ with $T=t = 0.125$ and the band filling $\text{hni} = 0.90$. Also shown is the frequency dependence of the normalized spin susceptibility $2 \langle Q; !_m \rangle = [\langle Q; 0 \rangle + \langle Q; 2T \rangle]$ for $Q = (\pi; 0)$.

- ¹⁴ R. Preuss, W. Hanke, and W. von der Linden, Phys. Rev. Lett. 75, 1344 (1995).
- ¹⁵ A. Moreo, S. Haas, A. W. Sandvik, and E. Dagotto, Phys. Rev. B 51, 12045 (1995).
- ¹⁶ T. Maier, M. Jarrell, T. Pruschke, and M. Hettler, Rev. Mod. Phys. 77 1027 (2005).
- ¹⁷ J. E. Hirsch and R. M. Fye, Phys. Rev. Lett. 56 2521 (1986).
- ¹⁸ M. Jarrell, Th. Maier, C. Huscroft and S. Moukouri, Phys. Rev. B 64, 195130 (2001).
- ¹⁹ N. Bulut, D. J. Scalapino, and S. R. White, Phys. Rev. B 47, 14599 (1993).
- ²⁰ D. J. Scalapino and S. R. White, Physica C 341, 367 (2000).
- ²¹ E. P. Lekhanov, F. Becca, and S. Sorella, Phys. Rev. B 71, 64511 (2005).